JAAS

Accepted Manuscript

This is an *Accepted Manuscript*, which has been through the Royal Society of Chemistry peer review process and has been accepted for publication.

Accepted Manuscripts are published online shortly after acceptance, before technical editing, formatting and proof reading. Using this free service, authors can make their results available to the community, in citable form, before we publish the edited article. We will replace this *Accepted Manuscript* with the edited and formatted *Advance Article* as soon as it is available.

You can find more information about *Accepted Manuscripts* in the Information for Authors.

Please note that technical editing may introduce minor changes to the text and/or graphics, which may alter content. The journal's standard Terms & Conditions and the Ethical guidelines still apply. In no event shall the Royal Society of Chemistry be held responsible for any errors or omissions in this *Accepted Manuscript* or any consequences arising from the use of any information it contains.

ROYAL SOCIETY OF CHEMISTRY

www.rsc.org/jaas

Cite this: DOI: 10.1039/c0xx00000x

www.rsc.org/xxxxxx

ARTICLE TYPE

Laser-Induced Breakdown Spectroscopy Using Laser Pulses Delivered by Optical Fibers for Analyzing Mn and Ti Elements in Pig Iron

Qingdong Zeng, Lianbo Guo, Xiangyou Li,* Chao He, Meng Shen, Kuohu Li, Jun Duan, Xiaoyan Zeng, and Yongfeng Lu

Received (in XXX, XXX) Xth XXXXXXXXX 20XX, Accepted Xth XXXXXXXXX 20XX
DOI: 10.1039/b000000x

A portable fiber-optic laser-induced breakdown spectroscopy (FO-LIBS) system was developed and employed to quantitatively analyze Mn and Ti elements in pig iron. The ablated craters produced by FO-LIBS are shallower with flatter bottom surfaces as compared with those produced by a conventional LIBS system without using optical fibers to deliver the laser pulses. This is beneficial on the special occasions requiring shallower destruction. The time-resolved images of plasma plumes were obtained and compared using both LIBS systems. Plasmas with lower temperature and electron density generated by the FO-LIBS system were thinner and more uniform, which means a lower self-absorption. Using the FO-LIBS system, the coefficients of determination (R^2 factors) of calibration curves for Mn and Ti elements were 0.997 and 0.998, respectively. The leave-one-out cross-validation (LOOCV) method was used to evaluate the detection accuracy. The root-mean-square error of cross-validation (RMSECV) for Mn (concentration range 0.072 - 2.06 wt.%) and Ti (concentration range 0.006 - 0.399 wt.%) elements were 0.0501 and 0.0054 wt.%, respectively. These results are comparable with or even slightly better than those obtained by the conventional LIBS. Furthermore, the FO-LIBS system is more compact and cost effective, more suitable for harsh environments, and hence more promising for industrial applications.

1. Introduction

Laser-induced breakdown spectroscopy (LIBS) is a technique for element analyses in which a laser pulse ablates a sample to generate plasmas, and the optical emission from the plasmas is collected and analyzed.[1-4] LIBS has proven to be a versatile analytical technique during past decades[5-7] due to its unique features, including applicability to any type of samples, no or simple sample preparation, nearly nondestructive nature, simultaneous multi-element detection, standoff sensing capability, and rapid in situ analyses, etc.[8-10] These advantages offer a wide range of potential applications in fields such as environmental science, biotechnology, industry, agriculture, combustion, and defense.[11-15] However, the conventional LIBS (without using optical fibers to deliver the laser pulses)[16-18] is limiting when the environment is too aggressive or the access restriction makes it difficult to produce plasmas or acquire the emission lines.[19-20] It is often large, complex, and expensive, limiting its use in laboratory investigation and making it unsuitable for large-scale industrial applications or in extreme environments.

Fiber-optic, laser-induced breakdown spectroscopy (FO-LIBS) provides a solution to the problems mentioned above because its laser beam can conveniently be delivered to the target surfaces using an optical fiber.[3,17, 20–22] In recent years, FO-LIBS has been studied by several groups. Davies *et al.* [23] utilized FO-LIBS to successfully detect metallic species in the hostile environments of nuclear reactor buildings. Gruber *et al.* [8,24] utilized FO-LIBS to analyze liquid steel at a distance of 1.5 m and quantitatively detect the major elements in an industrial mineral melt at a temperature between 1400 and 1600 °C. Whitehouse *et al.*[25] used a 75 m-long umbilical FO-LIBS system to determine the copper content of 316H austenitic stainless steel superheated bifurcation tubing within the pressure vessels of nuclear power stations. They obtained an accuracy of approximately 25% and a limit of detection (LOD) of 360 ppm over a range of 0.04% < Cu < 0.6% (by mass) with a measurement time per bifurcation of less than 3 min. Rai *et al.*[16,17,26] designed a FO-LIBS device aimed at online analysis of molten aluminum. Recently, Bohling *et al.*[27] reported on a FO-LIBS sensor with a microchip laser for detection of explosives and landmines on the surface of materials. Neural networks were used to improve the identification accuracy. Dumitrescu *et al.*[18] reported on a fiber that optically transmits laser spark for fuel-to-air ratio measurements in ultra-lean methane air mixtures. The LIBS signals acquired from the fiber-optically generated plasmas showed a linear dependence on the H/N ratio.

Recently, a further fast growing laser technology that seems to be very promising for LIBS (particularly in industrial applications) was represented by the high power pulsed fiber lasers.[28] Fiber lasers, with higher photon conversion efficiency and a compact size (which is an important requirement for reducing the overall dimensions of portable LIBS systems), are a variation of the standard solid-state lasers where the active

medium is an optical fiber rather than a rod.[28] Scharun et al. [29] reported a multi-kHz fiber laser for mobile metal analysis tasks. The achieved accuracy is similar or even better than the state-of-the-art mobile SD-OES system for the described concentrations ranges and measurement conditions. However, due to the high PRF (pulse repetition frequency), it is not easy to collect the spectra generated by each single pulse using a compact spectrometer coupled with a CCD detector.

It is worth mentioning that, there are also several especial LIBS systems of state-of-the-art successful applied in harsh environment without using fiber optic to delivery laser beam; e. g. Sturm *et al.* [30] used an automated LIBS system for the inline analysis of liquid slag with temperatures from ≈600 to ≈1400 ℃ within 2 min in the ladle of a slag transporter. However, the large equipment was used in a specific situation, and it was not easy to move conveniently as a mobile or portable device.

The works described above provided versatile approaches and obtained good results for FO-LIBS and other LIBS configuration. However, few researchers have compared FO-LIBS and conventional LIBS to study the benefit of the uniform laser beam profiles of the FO-LIBS to the quantitative analyses of elements in LIBS.

In this work, a portable FO-LIBS system was developed for analyzing Mn and Ti elements in pig iron. The leave-one-out cross-validation method was used to evaluate the accuracy of the quantitative analyses. The surface morphology of the pig iron samples produced by FO-LIBS was examined using an optical microscope and a step profiler. The time evolution of the plasma plumes was observed by fast imaging using an intensified charge-coupled device (ICCD). The temperature and electron density of the plasma were evaluated.

2. Experimental setup and methodology

2.1 Experimental setup

The schematic diagram of the FO-LIBS setup is shown in Fig. 1 (a). A compact Q-switch Nd:YAG pulsed laser (wavelength: 532 nm, pulse duration: 7 ns, repetition rate: 10 Hz) was employed. Transmitted through a 3 m-long optical fiber (core diameter: 1 mm) and reflected by a dichroic mirror, the laser beam was focused onto the sample surface by a UV-grade quartz lens with a focal length of 150 mm. The plasma spectrum was collected by a compact spectrometer (AvaSpec-2048-USB2, 75mm Czerny-Turner, grating: 2400 lines/mm (VE), slit: 10 µm, spectral resolution: about 0.08 nm, spectral range: approx. 393 to 488 nm), coupled with a gated linear CCD detector with 2048 elements and synchronized by the external trigger of the laser. Before recording a spectrum, the processing parameters were optimized and fixed as follows. The laser pulse energy measured under the focusing lens was about 24 mJ, which is limited by the optical fiber delivered laser pulses. The focal point was set at 1 mm below the sample surface. The estimated fluence was about 3.1 *J/cm*^{2}. Prior to the acquisition, a number of pulses were applied to eliminate the surface contamination. The acquisition began at 1.3 µs after the laser pulse with an integration time of 2 ms. Every measurement in the experiments was repeated ten times unless specified.

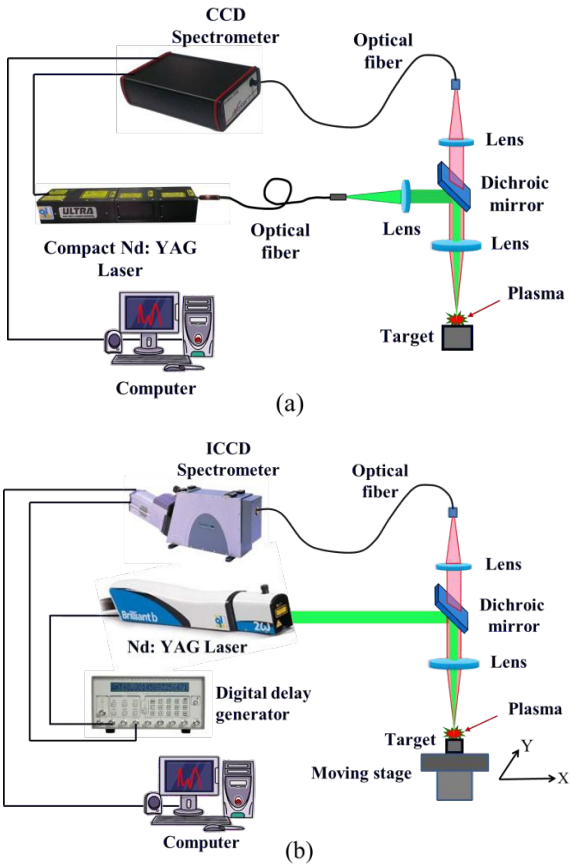

Fig. 1. Schematic diagrams of the FO-LIBS (a) and conventional LIBS (b) systems.

The schematic diagram of the conventional LIBS system is shown in Fig. 1 (b). The difference from the FO-LIBS setup is that a Q-switched Nd: YAG laser (Quantel Ltd. Brilliant B, 532 nm, 6 ns, 10 Hz) and an echelle spectrometer (Andor Tech, ME5000, spectral range from 200 nm to 950 nm, resolution λ/Δλ=5000) coupled with an ICCD camera (Andor Tech, iStar DH334T) were used in the system. Both the laser and the ICCD camera were synchronized by a digital delay generator (Stanford Research System DG535). A computer-controlled platform was used to move the samples. The processing parameters were optimized and fixed as followed: laser pulse energy was 50 mJ measured under the focusing lens. The focal point was under the sample's surface at a depth of 4 mm. The estimated laser fluence was about 25.5 J/cm^2. The gate delay time and width of the ICCD were 4 and 20 µs, respectively.

2.2 Samples

Seven certified pig iron samples (GSB 03-2582-2010 series, Pangang Group Research Institute Co. Ltd) were used in this work. The matrix elements in all of these samples were iron with a content of over 90%. The concentrations of the Mn and Ti elements are listed in Table 1.

Table 1. Reference concentrations of Mn and Ti elements in the pig iron samples (wt.%).

No.	1#	2#	3#	4#	5#	6#	7#
Mn	0.072	0.329	1.22	0.857	0.596	1.46	2.06
Ti	0.0059	0.216	0.043	0.03	0.066	0.105	0.399

3. Results and discussion

3.1 Characterization of laser-produced craters

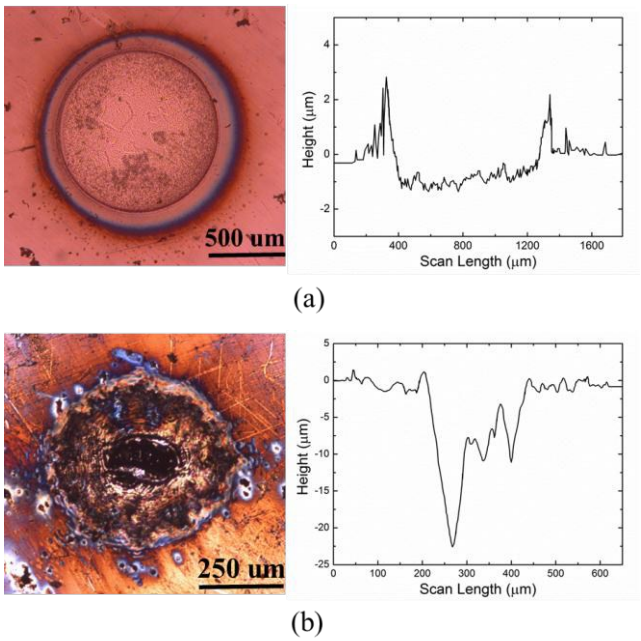

Fig. 2. Optical micrographs and depth profiles of pig iron samples irradiated by 20 laser pulses: (a) FO-LIBS with a laser fluence of 3.1 J/cm^2 and (b) conventional LIBS with a laser fluence of 25.5 J/cm^2.

The surface morphology of the pig iron samples produced by FO-LIBS was examined using an optical microscope and a step profiler. Figure 2 (a) shows the effect of 20 laser pulses with a fluence of 3.1 J/cm^2 on the sample surface in the FO-LIBS, while Fig. 2 (b) shows the effect of 20 laser pulses with a fluence of 25.5 J/cm^2 on the sample surface in the conventional LIBS.

The crater morphology produced by FO-LIBS was significantly different from that by conventional LIBS. The depth of craters (approximately 1 μm) by FO-LIBS was much shallower than that by conventional LIBS (approximately 22 μm). Therefore, FO-LIBS causes much less surface damage. Furthermore, the bottom of the craters produced by the FO-LIBS were much flatter than those made by the conventional LIBS, possibly caused by the different laser energy and beam quality, suggesting that the laser distribution in the FO-LIBS is more uniform than that of the conventional LIBS.

The characteristics of laser-produced craters in FO-LIBS (shallower and flatter) are beneficial on the special occasions requiring shallower destruction, such as film depth profile examination, quality controlling of coating.

3.2 Fast imaging of laser-induced plasmas

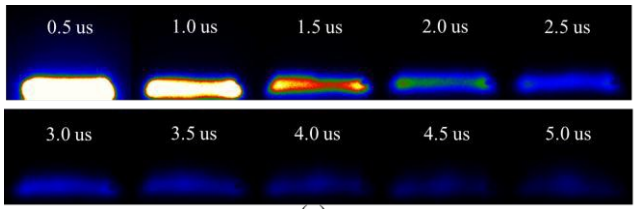

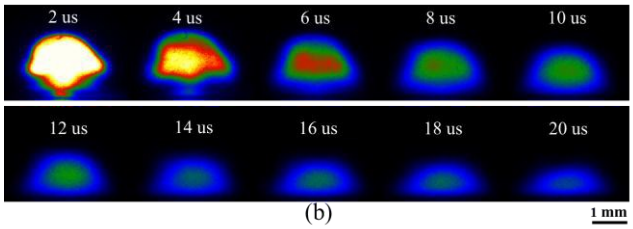

Fig. 3. Fast images of laser-induced plasmas in the FO-LIBS (a) and the conventional LIBS (b).

To further study the characteristics of FO-LIBS, the temporal evolution of the plasma plumes was observed using fast imaging, as shown in Fig. 3. These images were acquired using an Andor ICCD (iStar DH334T) attached with a Nikon lens (105 mm, f/2.8G). Each image was obtained by accumulating for ten pulses. The pictures showed that the plasmas generated by FO-LIBS were uniform, thinner, and plate-shaped, which was much different from that generated by conventional LIBS.

In addition, the lifetime of the plasmas generated by FO-LIBS is very short (approximately 5 μs, beyond this delay time, the intensity of the plasma became too weak to be measured), while that by conventional LIBS is much longer (estimated at more than 20 μs).

3.3 Temperature and electron density of plasmas

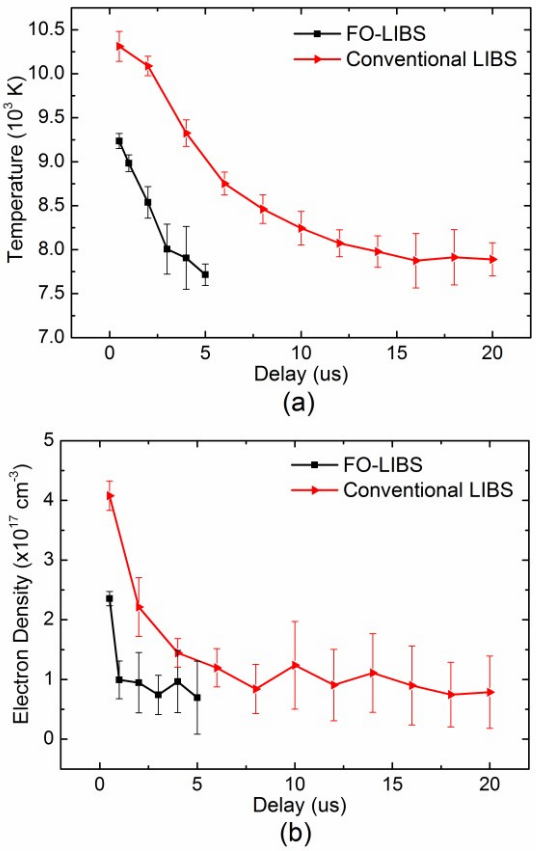

Fig. 4. The temperatures (a) and the electron densities (b) of laser-produced plasmas obtained in the FO-LIBS and conventional LIBS.

By Boltzmann plot method, [1] excitation temperature was estimated using iron atomic lines. [1, 31] Temporal evolution of

plasma temperatures in the FO-LIBS and the conventional LIBS are shown in Fig. 4 (a). The temperature of the produced plasma was determined up to 5 μs in the FO-LIBS and 20 μs in the conventional LIBS after the laser pulse. Beyond this delay, the emission of the iron lines used for the calculation became too weak to be measured with adequate precision. The results show that the temperature of plasmas in the FO-LIBS is lower than that of conventional LIBS at a certain delay. In addition, the temperature decline rapidly and the total plasma emission lifetime is about 4–5 μs. These are consistent with the temporal evolution of the plasma plumes stated above.

By the Stark broadening method, the electron density of the laser-induced plasma was calculated by the following formula: [1,32]

$$\Delta\lambda_{Stark} = W_{FWHM}\left(\frac{n_e}{10^{16}cm^{-3}}\right), \quad (1)$$

Where $\mathbf{\Delta\lambda_{Stark}}$ is the full width at half maximum (FWHM) of the line, $\mathbf{W_{FWHM}}$ is the Stark broadening parameter for the full width (FWHM), and $\mathbf{n_e}$ is the electron density. The ionic line of aluminum at 394.40 nm was used to evaluate the plasma electron density and the procedure was described in ref. 1,3,32. Temporal evolution of electron density of plasmas generated in the FO-LIBS and the conventional LIBS are shown in Fig. 4 (b). It shows that the electron density in the FO-LIBS is lower than that of conventional LIBS at a certain delay. This is consistent with the time evolution of the plasma temperatures stated above, suggesting that the plasma in the FO-LIBS is weaker than that of the conventional LIBS.

3.4 Qualitative and quantitative analyses

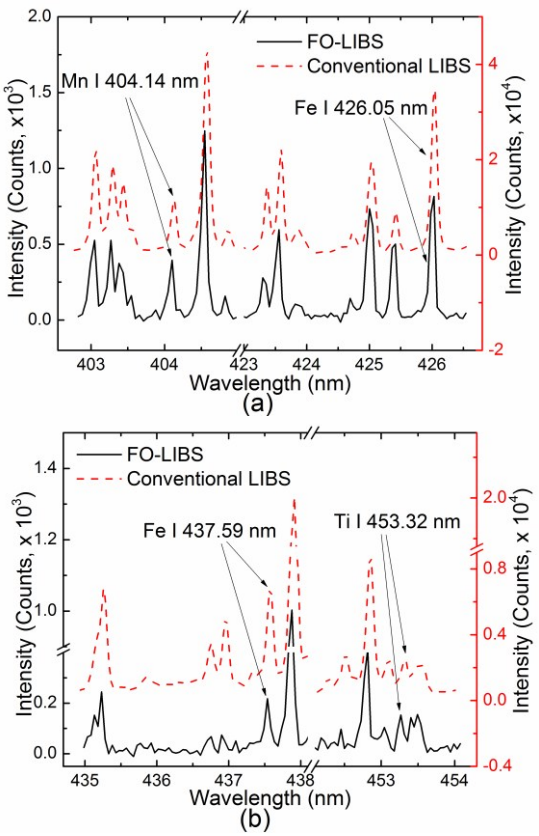

Fig. 5. The characteristic emission spectra of Mn (a) and Ti (b) elements obtained by the FO-LIBS and conventional LIBS.

The emission spectra of Mn and Ti elements acquired by both FO-LIBS and conventional LIBS are shown in Fig. 5. All of the spectra were acquired from Sample 6. As shown in Fig. 5, there is no obvious difference in the spectra acquired by FO-LIBS and conventional LIBS except the intensity.

The internal standardization, which used intensity ratio (analyte/reference line) instead of absolute peak heights to construct the calibration curve, was adopted as the quantitative analysis method. It has advantages such as minimizing shot-to-shot variations in the LIBS emission signals, increasing measurement precision.[1,3,8] To avoid interference, the spectrum lines of Mn I 404.14 nm and Ti I 453.32 nm were chosen as the analysis spectral lines. The matrices Fe I 426.05 nm and Fe I 437.59 nm were adopted as the reference lines.

Quantitative analyses of Mn and Ti elements were carried out using both FO-LIBS and conventional LIBS. The calibration curve for intensity ratios of Mn I 404.14 nm/Fe I 426.05 nm and Ti I 453.32 nm/Fe I 437.59 nm were established, as shown in Fig. 6 (a) and (b), respectively. The coefficients of determination (R^2 factors) of the calibration curves for FO-LIBS and conventional LIBS are listed in Table 2.

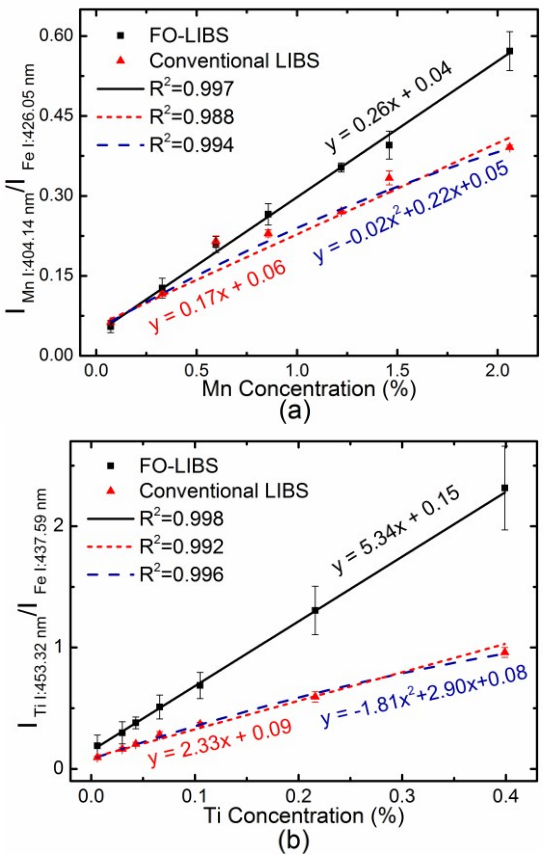

Fig. 6. Calibration curves for intensity ratios of Mn I 404.14 nm/Fe I 426.05 nm (a) and Ti I 453.32 nm/Fe I 437.59 nm (b) in FO-LIBS and conventional LIBS.

The limit of detection (LOD) can be calculated using the following equation: [1,3,33]

$$LOD = 3\sigma_a/k, \quad (2)$$

where σ_a is the average standard deviation of the noise and k is the slope of the calibration curve. However, in the internal standardization, the slope is the ratio of intensity

(analyte/reference line) to concentration, so Formula (2) can be transformed into the following:

$$\mathrm{LOD} = 3\sigma_a / I_R / \mathrm{S}, \quad (3)$$

where I_R is the intensity of the reference lines and S is the slope of the calibration curve using the internal standard method. According to Eq (3), the LOD is inversely proportional to I_R. The LOD of Mn and Ti in the pig iron samples of both LIBS systems were calculated and are shown in Table 2.

Furthermore, the leave-one-out cross-validation method was used to evaluate the detection accuracy. The root mean square error of cross-validation (RMSECV) was used as the main index for evaluating the performance of the calibration model. RMSECV is the average error in the calibration (validation) model and can be calculated by [1, 33]

$$RMSEC(V) = \sqrt{\frac{\sum_{i=1}^{n} (x_i - \hat{x}_i)^2}{n}}, \quad (4)$$

where $\hat{x}_i$ is the reference concentration of the sample, x_i is the predicted concentration of the sample, and n is the number of calibration (validation) samples. According to Eq (4), the RMSECV of calibration model for Mn and Ti in both LIBS systems were calculated and are listed in Table 2.

Table 2. The R-square (R^2) factor, RMSECV (wt.%), and the LODs of Mn and Ti elements in FO-LIBS and conventional LIBS.

Elements	R^2		RMSECV (wt.%)		LOD (ppm)	
	FO-LIBS	Conventional LIBS	FO-LIBS	Conventional LIBS	FO-LIBS	Conventional LIBS
Mn	0.997	0.988	0.0501	0.1793	1219	155
Ti	0.998	0.992	0.0054	0.0159	257	29

As shown in Table 2, both the R-square (R^2) factor and the RMSECV of FO-LIBS were comparable with or even slightly better than those of conventional LIBS, which suggests that the accuracy of FO-LIBS is comparable with or even slightly better than that of conventional LIBS. This is due to self-absorption whose effect influences the LIBS measurements, reflecting in non-linear calibration curves. [1,3,34] As shown in Fig. 6, there are nonlinear behaviors occurred in calibration curves of the conventional LIBS.

The self-absorption generally increases with the electron density and the optical thickness of plasma. [34] Because of the high density of atoms in the plasma and its characteristically high temperature and electron density gradients, the outer layer of the plasma will be populated by 'cool' atoms, residing mostly in the ground state. [35] The central core of the plasma will contain a higher density of excited atoms. As these atoms decay to the ground state, the emitted photons corresponding to resonance transitions will have a high probability of being absorbed by the 'cooler' atoms in the outer layers, [35] which would influence the result of analysis. In addition, with higher laser intensity, it is more probable to occur self-absorption of the emission by the plasma formed in front of the sample, or due to poor coupling of the laser because of plasma shielding.[3] However, the plasmas generated in FO-LIBS are thinner, weaker, and more uniform, as well as the temperature and electron density are lower than that in conventional LIBS, which may lead to less self-absorption or self-reversal for emission line. These are probable reasons to explain the R-square (R^2) factor and the RMSECV (wt.%) in the FO-LIBS were a little better than that of the conventional LIBS.

However, the LODs in the FO-LIBS are inferior to that of the conventional LIBS and other LIBS systems (e.g. LoD (Mn) =9 ug/g with multiple pulse excitation in the vacuum ultraviolet,[36] and LoD (Mn) =4 ug/g using multi-pulse bursts in argon gas.[37]), which may be caused by the weak spectrum intensity. Due to the fiber limitation, the laser energy of the FO-LIBS is smaller than that of the conventional LIBS, which resulted that the intensity of the spectral line is weaker than that of the conventional LIBS. From Formula (2), the intensity of the reference line in FO-LIBS is much smaller than that in conventional LIBS. Namely, $\boldsymbol{I_R}$ is much smaller, so that the LODs of FO-LIBS are higher.

4. Conclusions

In summary, a compact and low-cost FO-LIBS system was developed for quantitative analyses of Mn and Ti elements in pig iron. The laser-produced craters of FO-LIBS are shallower and flatter than those obtained by conventional LIBS, which is beneficial on the special occasions requiring shallower destruction, such as film depth profile examination, quality controlling of coating. The plasmas generated in FO-LIBS are thinner, weaker, and more uniform, with the temperature and the electron density are lower than those in conventional LIBS, which probably leads to less self-absorption or self-reversal for emission line. The coefficients of determination (R^2 factors) of the calibration curves in FO-LIBS for Mn and Ti elements are 0.997 and 0.998, respectively. The RMSECV (wt.%) for Mn and Ti elements are 0.0501 and 0.0054 wt.%, respectively. These results are comparable with or even slightly better than those obtained by conventional LIBS, although the LOD of FO-LIBS is slightly inferior to conventional LIBS. However, compared to the conventional LIBS system, the FO-LIBS system is more compact and cost effective (CCD systems are more cost effective and robust than ICCDs [38]). FO-LIBS is a convenient approach to providing a portable solution for LIBS applications in harsh or other special environments.

Acknowledgement

This work was financially supported by the National Special Fund for the Major Scientific Instrument and Equipment Development Project (No. 2011YQ160017) of China, by the National Natural Science Foundation of China (No. 51429501), and by the Fundamental Research Funds for the Central Universities of China (HUST: CXY13Q022).

Notes and references

Wuhan National Laboratory for Optoelectronics (WNLO), Huazhong University of Science and Technology (HUST), Wuhan, Hubei 430074, P.R. China. Fax: 86-27-87541423; Tel: 86-27-87541423; E-mail: xyli@mail.hust.edu.cn

1. R. Noll, *Laser-Induced Breakdown Spectroscopy*, Springer. 2012.
2. O. A. Nassef and H. E. Elsayed-Ali, *Spectrochimica Acta Part B: Atomic Spectroscopy*, 2005, **60**, 1564-1572.
3. J. P. Singh and S. N. Thakur, *Laser-induced breakdown spectroscopy*, Elsevier. 2007.
4. D. A. Cremers and R. C. Chinni, *Applied Spectroscopy Reviews*, 2009, **44**, 457-506.
5. C. M. Li, Z. M. Zou, X. Y. Yang, Z. Q. Hao, L. B. Guo, X. Y. Li, Y. F. Lu and X. Y. Zeng, *Journal of Analytical Atomic Spectrometry*, 2014, **29**, 1432-1437. DOI: 10.1039/C4JA00036F.
6. J.-F. Gravel, F. Doucet, P. Bouchard and M. Sabsabi, *Journal of Analytical Atomic Spectrometry*, 2011, **26**, 1354-1361.
7. A. Giakoumaki, K. Melessanaki and D. Anglos, *Analytical and bioanalytical chemistry*, 2007, **387**, 749-760.
8. D. W. Hahn and N. Omenetto, *Applied Spectroscopy*, 2012, **66**, 347-419.
9. L. Guo, B. Zhang, X. He, C. Li, Y. Zhou, T. Wu, J. Park, X. Zeng and Y. Lu, *Optics express*, 2012, **20**, 1436-1443.
10. L. Liu, S. Li, X. He, X. Huang, C. Zhang, L. Fan, M. Wang, Y. Zhou, K. Chen and L. Jiang, *Optics express*, 2014, **22**, 7686-7693.
11. J. Carranza, B. Fisher, G. Yoder and D. Hahn, *Spectrochimica Acta Part B: Atomic Spectroscopy*, 2001, **56**, 851-864.
12. A. Kumar, F.-Y. Yueh, J. P. Singh and S. Burgess, *Appl. Optics*, 2004, **43**, 5399-5403.
13. M. D. Mowery, R. Sing, J. Kirsch, A. Razaghi, S. Béchard and R. A. Reed, *Journal of pharmaceutical and biomedical analysis*, 2002, **28**, 935-943.
14. K. Y. Yamamoto, D. A. Cremers, M. J. Ferris and L. E. Foster, *Applied spectroscopy*, 1996, **50**, 222-233.
15. Z. Wang, T.-B. Yuan, Z.-Y. Hou, W.-D. Zhou, J.-D. Lu, H.-B. Ding and X.-Y. Zeng, Frontiers of Physics, 2014, 1–19.
16. A. K. Rai, H. Zhang, F. Y. Yueh, J. P. Singh and A. Weisburg, *Spectrochimica Acta Part B: Atomic Spectroscopy*, 2001, **56**, 2371-2383.
17. C. Pasquini, J. Cortez, L. Silva and F. B. Gonzaga, Journal of the Brazilian Chemical Society, 2007, 18, 463-512.
18. C. Dumitrescu, P. Puzinauskas, S. Olcmen, S. G. Buckley, S. Joshi and A. P. Yalin, *Applied spectroscopy*, 2007, **61**, 1338-1343.
19. G. A. Theriault, S. Bodensteiner and S. H. Lieberman, *Field Analytical Chemistry & Technology*, 1998, **2**, 117-125.
20. F. Anabitarte, A. Cobo and J. M. Lopez-Higuera, *ISRN Spectroscopy*, 2012, 2012, 12. DOI: 10.5402/2012/285240.
21. B. J. Marquardt, S. R. Goode and S. M. Angel, *Analytical Chemistry*, 1996, **68**, 977-981.
22. D. Cremers, J. Barefield and A. Koskelo, *Applied Spectroscopy*, 1995, **49**, 857-860.
23. C. Davies, H. Telle, D. Montgomery and R. Corbett, *Spectrochimica Acta Part B: Atomic Spectroscopy*, 1995, **50**, 1059-1075.
24. J. Gruber, J. Heitz, H. Strasser, D. Bäuerle and N. Ramaseder, *Spectrochimica Acta Part B: Atomic Spectroscopy*, 2001, **56**, 685-693.
25. A. Whitehouse, J. Young, I. Botheroyd, S. Lawson, C. Evans and J. Wright, *Spectrochimica Acta Part B: Atomic Spectroscopy*, 2001, **56**, 821-830.
26. A. K. Rai, F.-Y. Yueh and J. P. Singh, *Appl. Optics*, 2003, **42**, 2078-2084.
27. C. Bohling, D. Scheel, K. Hohmann, W. Schade, M. Reuter and G. Holl, *Appl. Optics*, 2006, **45**, 3817-3825.
28. S. Musazzi and U. Perini, Laser-Induced Breakdown Spectroscopy: Theory and Applications, Springer. 2014.
29. M. Scharun, C. Fricke-Begemann and R. Noll, *Spectrochimica Acta* Part B: Atomic Spectroscopy, 2013, 87, 198-207.
30. V. Sturm, R. d. Fleige, M. de Kanter, R. Leitner, K. Pilz, D. Fischer, G. Hubmer and R. Noll, Analytical chemistry, 2014.
31. Z. Hao, L. Guo, C. Li, M. Shen, X. Zou, X. Li, Y. Lu and X. Zeng, J. Anal. At. Spectrom., 2014, 29, 2309-2314.
32. H. Griem, Spectral Line Broadening by Plasmas, Academic, New York, 1997.
33. S. Yao, J. Lu, M. Dong, K. Chen, J. Li and J. Li, *Applied spectroscopy*, 2011, **65**, 1197-1201.
34. F. Bredice, F. Borges, H. Sobral, M. Villagran-Muniz, H. Di Rocco, G. Cristoforetti, S. Legnaioli, V. Palleschi, L. Pardini and A. Salvetti, Spectrochimica Acta Part B: Atomic Spectroscopy, 2006, 61, 1294-1303.
35. Cremers, David A., and Leon J. Radziemski. Handbook of Laser–Induced Breakdown Spectroscopy, 2006.
36. V. Sturm, L. Peter and R. Noll, Applied Spectroscopy, 2000, 54, 1275-1278.
37. V. Sturm, J. Vrenegor, R. Noll and M. Hemmerlin, J. Anal. At. Spectrom., 2004, 19, 451-456.
38. H. Heilbrunner, N. Huber, H. Wolfmeir, E. Arenholz, J. Pedarnig and J. Heitz, Spectrochimica Acta Part B: Atomic Spectroscopy, 2012, 74, 51-56.